^{18}F-PFPN PET: A New and Attractive Imaging Modality for Patients with Malignant Melanoma

Xiao Zhang*[1,2], Mengting Li*[1,2], Yongkang Gai[1,2], Jing Chen[3], Juan Tao[4], Liu Yang[4], Fan Hu[1,2], Wenyu Song[1,2], Tzu-Chen Yen[5,6], and Xiaoli Lan[1,2]

[1]*Department of Nuclear Medicine, Union Hospital, Tongji Medical College, Huazhong University of Science and Technology, Wuhan, China;* [2]*Hubei Key Laboratory of Molecular Imaging, Wuhan, China;* [3]*Cancer Center, Union Hospital, Tongji Medical College, Huazhong University of Science and Technology, Wuhan, China;* [4]*Department of Dermatology, Union Hospital, Tongji Medical College, Huazhong University of Science and Technology, Wuhan, China;* [5]*Department of Medicine and Molecular Imaging Center, Linkou Chang Gung Memorial Hospital and Chang Gung University, Taoyuan City, Taiwan; and* [6]*Aprinoia Therapeutics Co., Ltd., Suzhou, China*

^{18}F-FDG PET has limited diagnostic applications in malignant melanoma (MM). ^{18}F-*N*-(2-(diethylamino)ethyl)-5-(2-(2-(2-fluoroethoxy)ethoxy)ethoxy)picolinamide (^{18}F-PFPN) is a novel PET probe with high affinity and selectivity for melanin. We conducted a clinical study with 2 aims, first to investigate the biodistribution and radiation dosimetry of ^{18}F-PFPN in healthy volunteers, and second, to examine the diagnostic utility of ^{18}F-PFPN PET imaging in patients with MM. **Methods:** ^{18}F-PFPN was synthesized through a fluoro-for-tosyl exchange reaction. Five healthy volunteers were enrolled to investigate the biodistribution, pharmacokinetics, radiation dosimetry, and safety of the tracer. Subsequently, a total of 21 patients with clinically suspected or confirmed MM underwent both ^{18}F-PFPN PET/MRI and ^{18}F-FDG PET/CT scans. The normalized SUV_{max} of selected lesions was determined for both tracers and compared in patient- and lesion-based analyses. **Results:** ^{18}F-PFPN has an elevated radiochemical yield and was highly stable in vivo. In healthy volunteers, ^{18}F-PFPN was safe and well tolerated, and its effective absorbed dose was comparable to that of ^{18}F-FDG. In patient-based analysis, ^{18}F-PFPN uptake was higher than ^{18}F-FDG for both primary tumors and nodal metastases. In lesion-based analysis,^{18}F-PFPN PET imaging could detect 365 metastases that were missed on ^{18}F-FDG PET. Additionally, ^{18}F-PFPN PET imaging had clinical value in distinguishing false-positive lesions on ^{18}F-FDG PET. **Conclusion:** ^{18}F-PFPN is a safe and well-tolerated melanin PET tracer. In a pilot clinical study, ^{18}F-PFPN PET imaging outperformed traditional ^{18}F-FDG PET in identifying both primary MM and its distant spread.

Key Words: ^{18}F-PFPN; ^{18}F-FDG; malignant melanoma; PET; diagnosis

J Nucl Med 2022; 63:1537–1543
DOI: 10.2967/jnumed.121.263179

Malignant melanoma (MM) is a highly aggressive tumor that poses a significant public health burden (*1*). The 5-y overall survival rates of patients with nodal and distant spread are as low as 65% and 25%, respectively. However, early surgical excision of localized MM portends favorable outcomes (5-y overall survival, 98%). In this scenario, both prompt diagnosis and accurate disease staging are paramount to reduce mortality.

Traditional ^{18}F-FDG PET may be clinically useful for staging and therapeutic monitoring of advanced (stage III−IV) MM (*2*). However, the value of ^{18}F-FDG PET imaging in this malignancy is limited by uptake in the liver and brain (*3*), which may ultimately compromise reliable detection of primary or metastatic melanoma lesions at these anatomic sites. Additionally, ^{18}F-FDG PET does not have sufficient sensitivity to diagnose stage I−II MM (*4*) and is generally unable to identify small (<1 cm) metastases to the lung, liver, and brain (*5*).

Recent advances in specific PET tracers, including MM-selective antibodies (*6,7*), α-melanocyte–stimulating hormone receptor ligands (*5,8*), and peptides (*9,10*), have fostered our ability to identify MM lesions. Unfortunately, several caveats, including slow and limited tumor uptake, suboptimal in vivo stability, and elevated liver accumulation, still hamper their routine clinical application. One of the most promising molecular targets for the imaging of MM is melanin, which exists in most melanomas (>90%) (*11*). Several melanin-targeted radiopharmaceuticals, including ^{123}I-MEL008 (*12*), ^{18}F-FBZA (*13*), ^{18}F-MEL050 (*14*), and 4-^{11}C-MBZA (*15*), have been synthesized from benzamide, quinoxaline, or picolinamide and applied as PET and SPECT tracers. We have previously designed and synthesized an ^{18}F-labeled benzamide analog as a melanin-imaging tracer, termed ^{18}F-5-fluoro-*N*-(2-[diethylamino]ethyl)picolinamide (^{18}F-5-FPN). This probe, characterized by high melanin affinity and favorable pharmacokinetic properties (*16,17*), has shown promising preclinical value for the identification of small (<2 mm) nodal and distant metastases from MM in mice (*18*). However, the relatively elevated hepatic tracer uptake of ^{18}F-5-FPN hindered its clinical applications. Subsequently, we optimized this probe to have a higher tumor–to–normal-liver ratio and radiochemical yield, named ^{18}F-*N*-(2-(diethylamino)ethyl)-5-(2-(2-(2-fluoroethoxy)ethoxy)ethoxy)picolinamide (^{18}F-PFPN) (*19*).

To shed further light on the translational value of ^{18}F-PFPN as a melanin-targeted PET probe for MM imaging, we designed the current study with 2 principal aims. First, we sought to investigate the biodistribution and radiation dosimetry of ^{18}F-PFPN in healthy volunteers. Second, we examined, for the first time, the clinical utility of ^{18}F-PFPN PET imaging in patients with suspected or pathologically confirmed MM.

Received Sep. 8, 2021; revision accepted Jan. 14, 2022.
For correspondence or reprints, contact Xiaoli Lan (LXL730724@hotmail.com).
*Contributed equally to this work.
Published online Feb. 3, 2022.

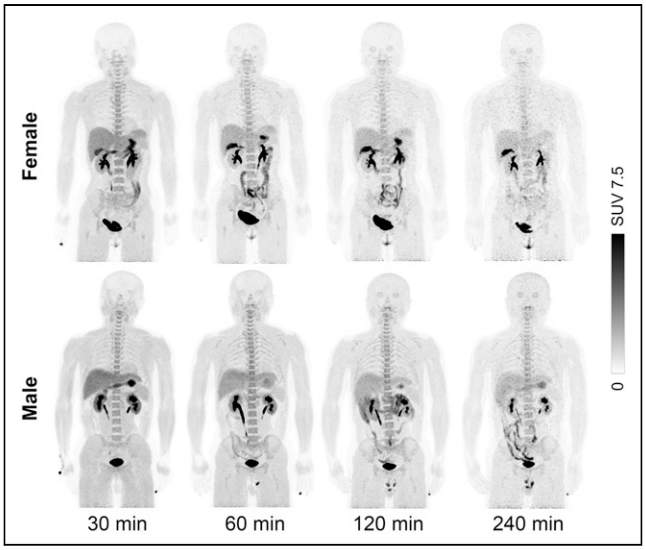

FIGURE 1. Maximum-intensity-projection PET images obtained from female and male volunteers at different time points after intravenous ^{18}F-PFPN injection.

MATERIALS AND METHODS

Healthy Volunteers and Patients

The institutional review board approved this study, and all subjects gave written informed consent. Five healthy volunteers (3 women and 2 men; age range, 28–48 y; Supplemental Table 1 [supplemental materials are available at http://jnm.snmjournals.org]) were enrolled to investigate the biodistribution, pharmacokinetics, radiation dosimetry, and safety of ^{18}F-PFPN. Between January 19, 2021, and June 19, 2021, the patients with clinically suspected or confirmed MM were recruited. All patients underwent ^{18}F-FDG PET/CT and ^{18}F-PFPN PET/MRI within 1 wk. CT was performed when MRI was contraindicated (1 patient because of a metal implant). Patients with acute systemic diseases, electrolyte disorders, other known malignancies, an age of less than 18 y, or pregnancy or lactation were then excluded.

Biodistribution and Radiation Dosimetry of ^{18}F-PFPN in Healthy Volunteers

^{18}F-PFPN was synthesized using the procedural steps outlined in Supplemental Figure 1 (*19*). The procedures for determining the tracer biodistribution and the radiation dosimetry are described in Supplemental Figure 2. In healthy volunteers, serial whole-body PET/MRI scans were subsequently acquired on an integrated PET/MRI scanner (Signa; GE

TABLE 1
General Characteristics of Patients with Clinically Suspected or Confirmed MM

Patient no.	Sex	Age (y)	Weight (kg)	^{18}F-PFPN dose (MBq)	^{18}F-FDG dose (MBq)	Clinical role of PET	Primary tumor location	Confirmed metastases*	Clinical stage/ final diagnosis
1	M	70	76	358.9	318.2	IS	Right plantar region	LNM, LM, BM, SM	T4bN3cM1, 4
2	F	55	54	270.1	244.2	IS	Left plantar region	LNM	T4bN3cM0, IIIc
3	M	40	73	344.1	314.5	IS	Left plantar region	—	T2bN0M0, IIa
4	M	47	55	214.6	259	RD	Occipital skin	LNM, GM	PD
5	M	67	59	196.1	266.4	IS	Right plantar region	LNM, LM, BM	T4bN3cM1, 4
6	M	59	69	266.4	281.2	RD	Left choroid (eye)	LM	PD
7	M	55	60	321.9	266.4	IS	Right plantar region	LNM, LM, BM	T4bN3cM1, 4
8	M	47	75	381.1	340.4	RD	Left choroid (eye)	LNM, LM, BM	PD
9	F	73	50	247.9	260.1	IS	Rectum	LNM, LM, BM, SM, PM	T4bN3cM1, 4
10	F	49	52	255.3	255.3	IS	Left isovarvas	LNM, BM	T3bN2bM1, 4
11	F	39	94	296	366.3	RD	Left pollex	LNM	PD
12	F	39	64	196.5	266.4	RD	Left plantar region	LNM	PD
13	F	63	60	303.4	273.8	RD	Right heel	LNM	PD
14	M	50	85	392.2	323.4	RD	Right plantar region	LNM, LM, BM, AM	PD
15	F	33	48	218.3	210.9	IS	Left arm	—	T4bN0M0, IIc
16	M	63	50	236.8	247.9	RD	Left heel	LNM, BM, PM, AM, CM, GM, CUM	PD
17	M	66	82	310.8	344.1	IS	Right forehead (skin)	LNM	T2aN2bM0, IIIb
18	F	54	60	247.9	259	RD	Perineum	LNM	PD
19	M	70	72	270.1	307.1	RD	Left plantar region	LNM	PD
20	F	50	67	270.1	254.2	RD	Left toe	LNM, PM, CUM	PD
21	F	63	67	314.5	259	RD	Perineum	LNM	PD

*Confirmed after thorough review of imaging and pathologic findings.

IS = initial staging; LNM = lymph node metastases; LM = liver metastases; BM = bone metastases; SM = spleen metastases; RD = recurrence detection; GM = gastric metastases; PD = progression of disease; PM = pulmonary metastases; AM = adrenal gland metastasis; CM = cerebral metastasis; CUM = cutaneous metastasis.

TABLE 2
Patient- and Lesion-Based Analyses of ^{18}F-PFPN and ^{18}F-FDG PET Imaging Findings

Analysis	Parameter	Primary tumor	Lymph node metastases	Bone metastases	Liver metastases	Metastases to other sites
Patient-based analysis		8	18	8	7	6
Number of patients	^{18}F-FDG	8	17	7	5	4
	^{18}F-PFPN	8	18	8	7	6
	P		1.0*	1.0*	0.462*	
Normalized SUV_{max}	^{18}F-FDG	4.42 ± 3.43	7.36 ± 6.08	6.18 ± 4.06	4.94 ± 4.36	13.92 ± 10.97
	^{18}F-PFPN, 1 h	10.27 ± 6.09	15.14 ± 14.07	18.21 ± 21.00	23.56 ± 25.66	20.32 ± 19.29
	^{18}F-PFPN, 3 h	17.82 ± 10.29	21.10 ± 17.66	28.47 ± 36.08	37.03 ± 48.64	29.87 ± 27.1
	P (1 h/3 h)	0.022*/0.008*	0.043/0.005	0.161/0.130	0.144/0.178	0.496/0.211
Lesion-based analysis			124	394	141	33
Number of lesions	^{18}F-FDG		98	151	49	29
	^{18}F-PFPN		124	394	141	33
	P		0.000	0.000	0.000	0.114†
Normalized SUV_{max}	^{18}F-FDG		5.36 ± 4.08	5.01 ± 2.33	5.08 ± 2.11	7.93 ± 7.70
	^{18}F-PFPN, 1 h		10.88 ± 9.49	20.14 ± 21.83	19.17 ± 17.29	11.97 ± 11.59
	^{18}F-PFPN, 3 h		16.35 ± 13.55	31.83 ± 37.09	31.55 ± 31.52	17.52 ± 16.56
	P (1 h/3 h)		0.000/0.000	0.000/0.000	0.000/0.000	0.117/0.006

*Paired *t* test.
†Fisher exact test.
1 h/3 h = *P* value calculated for ^{18}F-FDG SUV_{max} vs. ^{18}F-PFPN SUV_{max} at 1 or 3 h.

Healthcare) at 30, 60, 120, and 240 min after tracer injection. At each time point, images were acquired immediately after collection of biologic specimens (blood and urine). The tracer uptake in each major organ was determined by calculating the SUV_{mean}. The pharmacokinetic profile of ^{18}F-PFPN was investigated by determining the radioactive count of blood, plasma samples, and urine specimens collected at different time points using an automatic well-type automatic γ-counter (WIZARD 2470; PerkinElmer). The absorbed radiation dose for each major organ was calculated using the OLINDA/EXM software, version 2.1. The healthy volunteers were asked to report any subjective abnormality within 1 h from the completion of the study procedures. Vital signs were determined in the preprocedural phase and 4 h after tracer injection.

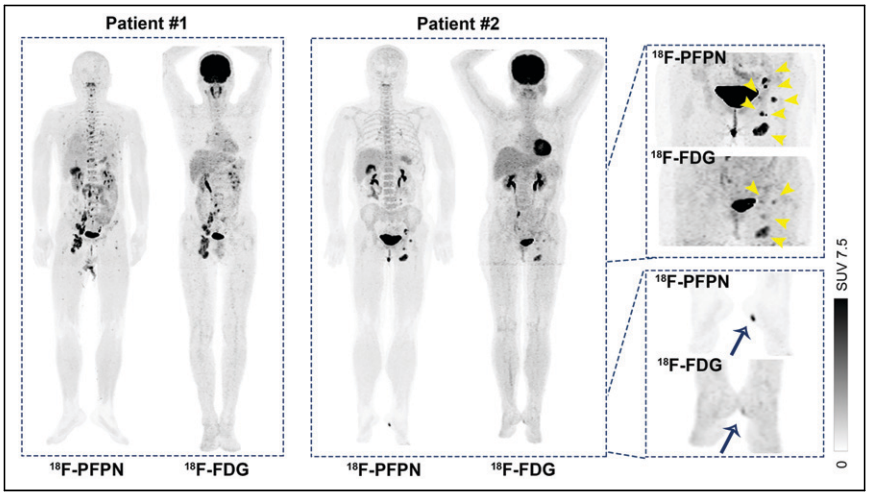

FIGURE 2. Representative images of patients with MM who underwent ^{18}F-PFPN and ^{18}F-FDG PET scans for disease staging. ^{18}F-PFPN PET outperformed traditional ^{18}F-FDG PET for identifying both primary tumors and distant metastases. Blue arrows indicate primary lesions, whereas yellow arrowheads denote lymph node metastases.

PET Imaging in Patients with Suspected or Pathologically Confirmed MM

^{18}F-PFPN PET/MR images were acquired approximately 1 and 3 h after the intravenous injection of ^{18}F-PFPN (dose, 3.0–5.4 MBq/kg). ^{18}F-FDG PET/CT images were acquired approximately 60 min after the intravenous injection of ^{18}F-FDG (dose, 3.7–5.4 MBq/kg). All scans were from the brain to the upper thigh (or the foot when required).

Image Interpretation

Images were uploaded on an Advantage Workstation (version AW4.6; GE Healthcare) for registration, fusion, and interpretation.

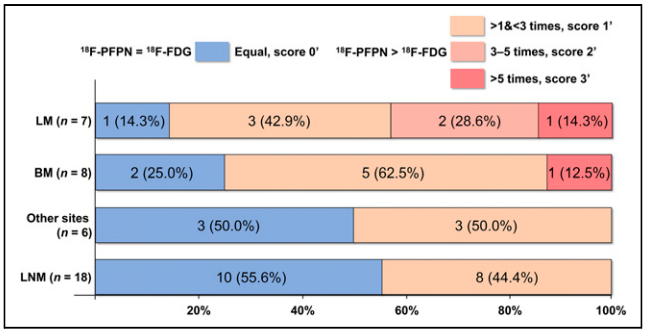

FIGURE 3. Comparative findings obtained from visual assessment of ^{18}F-PFPN and ^{18}F-FDG PET images. LM = liver metastases; BM = bone metastases; LNM = lymph node metastases. n (%) in each bar refers to patient number (patient number as a percentage of the total population).

^{18}F-PFPN and ^{18}F-FDG PET images were independently reviewed by 2 experienced nuclear medicine physicians who were not aware of patient clinical data and conventional imaging results. All discrepancies were resolved by consensus.

Regions of interest were drawn on transaxial slices, and the raw SUV_{max} was automatically calculated to quantify ^{18}F-FDG and ^{18}F-PFPN uptake within each lesion. To improve the comparability of SUV_{max}, raw data were normalized using the following formula:

$$\text{Normalized } SUV_{max} = \text{Raw } SUV_{max}/SUV_{bkgd},$$

where SUV_{bkgd} indicates the SUV_{mean} of the descending aorta.

Both patient- and lesion-based quantitative assessments were performed. Patient-based analysis included either the primary tumor or the single lesion showing the highest tracer uptake at each metastatic site. Lesion-based analysis for each site was performed either on all lesions (when their count was ≤10) or the 10 lesions that showed the highest tracer uptake (when their count was >10). A visual scoring system was also applied and is described in the supplemental materials.

Statistical Analysis

Continuous variables are presented as means ± SD. SUV_{max} was compared between groups using the Student *t* test. Categoric variables were compared using the χ^2 test. All analyses were undertaken in SPSS, version 22 (IBM). Two-tailed *P* values of less than 0.05 were considered statistically significant.

RESULTS

Quality Control and Radiochemistry of the ^{18}F-PFPN Tracer

^{18}F-PFPN was successfully synthesized. The radiochemical purity and specific activity of ^{18}F-PFPN (n = 5) was 97.38% ± 1.99% and 101–165 GBq/mmol, respectively. This probe's in vivo stability measured at 4 h after injection was more than 95%. An illustrative high-performance liquid chromatography image of the tracer in the urine is shown in Supplemental Figure 3.

Biodistribution, Dosimetry, and Safety of ^{18}F-PFPN in Healthy Volunteers

For healthy volunteers, the ^{18}F-PFPN maximum-intensity-projection images are shown in Figure 1. ^{18}F-PFPN uptake was visible in the renal pelvis and calices, ureters, gallbladder, urinary bladder, stomach, and liver. Hepatic SUV_{mean} decreased over time, being 4.51 ± 0.75, 3.26 ± 0.62, 2.45 ± 0.40, and 1.74 ± 0.28 at 30, 60, 120, and 240 min after injection, respectively (Supplemental Fig. 4). A similar pattern was observed for blood uptake, which gradually decreased from (2.65 ± 0.20) × 10^{-3} percentage injected dose [%ID]/g at 30 min after injection to (1.35 ± 0.67) × 10^{-3} %ID/g at 240 min (Supplemental Fig. 5). Comparable results were evident for most organs, except the gallbladder, eyes, and urine. The tracer activity in the urine was 0.15 ± 0.05 %ID/g at 30 min after injection and reached a peak of 0.35 ± 0.14 %ID/g at 60 min, suggesting rapid renal clearance. Concerning the eyes, we observed an SUV_{mean} increase from 0.79 ± 0.07 at 30 min after injection to 1.32 ± 0.30 at 240 min due to the presence of choroidal melanocytes and retinal pigment cells.

The estimated absorbed-radiation dosimetry for different organs is depicted in Supplemental Table. 2. The urinary bladder wall showed the highest dose activity (1.73 × 10^{-1} mSv/MBq), followed by the kidneys. A mean absorbed dose of 7.37 × 10^{-3} mSv/MBq was observed in the eyes. The total effective dose was 2.01 × 10^{-2} mSv/MBq.

Neither immediate adverse reactions nor significant changes in vital signs were observed after tracer injection. Similarly, follow-up laboratory examinations did not reveal any abnormal changes in liver and kidney function tests.

Characteristics of Patients with MM

In total, 21 patients (mean age, 54.86 ± 11.58 y) with clinically suspected or confirmed MM were included in the study (Table 1). Nine patients underwent imaging for initial disease staging, whereas investigations in the remaining 12 were aimed at detecting recurrences. Most primary MMs were in the skin, followed by choroid membranes. One patient had an occult primary MM located in the rectum.

Comparison of ^{18}F-PFPN and ^{18}F-FDG PET Imaging in Patients with MM

We subsequently compared ^{18}F-PFPN and ^{18}F-FDG PET imaging in MM patients (Table 2; Fig. 2). ^{18}F-PFPN PET could clearly delineate lesions, with an excellent

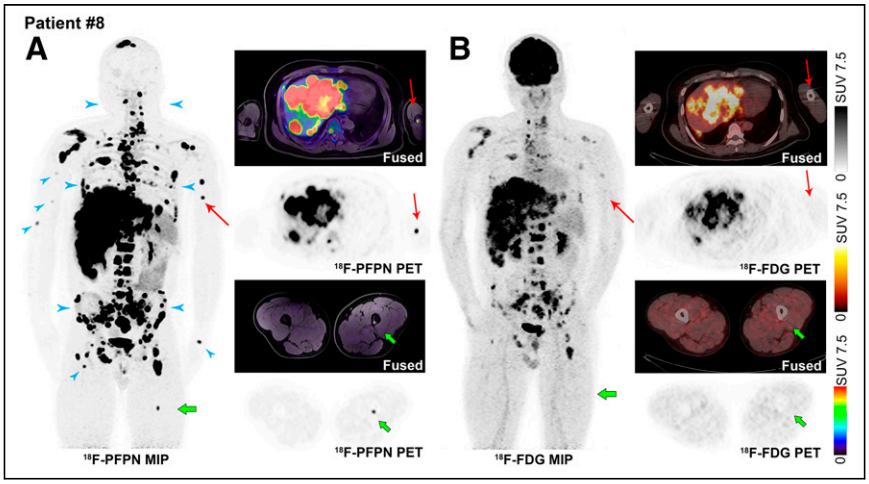

FIGURE 4. A 47-y-old man who underwent surgical removal of choroidal MM 19 mo before imaging. On maximum-intensity-projection (MIP) images, ^{18}F-PFPN PET (A) was able to identify higher number of lesions (blue arrowheads) than ^{18}F-FDG PET could (B). ^{18}F-PFPN PET/MRI identified hyperintense T1-weighted focus of increased tracer uptake in left arm (SUV_{max}, 8.4; red arrows) and left femur (SUV_{max}, 6.8; <2 mm, green arrows), which had normal uptake and density on ^{18}F-FDG PET/CT images.

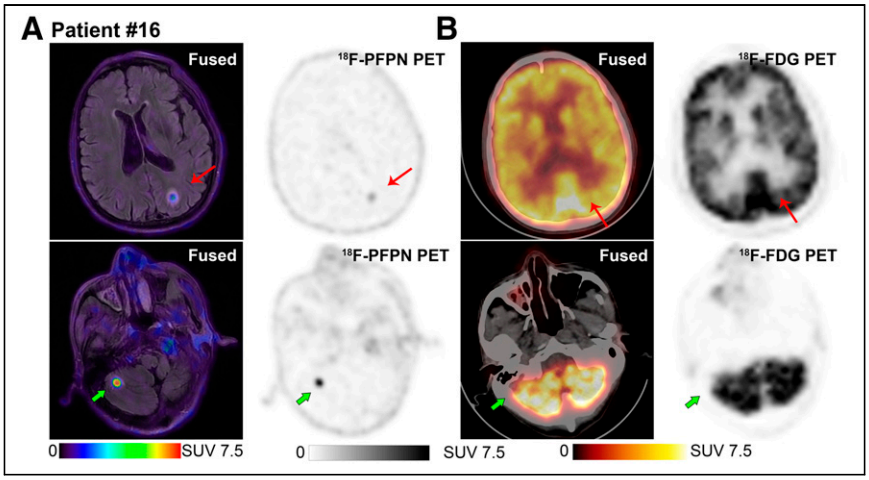

FIGURE 5. A 63-y-old man who underwent surgical removal of plantar melanoma 2 y before PET imaging. (A) Craniocerebral ^{18}F-PFPN PET/MRI revealed avid tracer uptake in left parietal lobe (SUV_{max}, 1.8; red arrows) and right cerebellum (SUV_{max}, 4.3; green arrows). (B) Conversely, no malignant lesions were visible on ^{18}F-FDG PET; notably, these images were characterized by high background activity caused by elevated physiologic tracer uptake in brain.

contrast due to low background uptake, especially in the brain and liver. On a patient-based analysis, both ^{18}F-PFPN and ^{18}F-FDG PET showed the same diagnostic performance (100%) for the detection of primary lesions; in addition, these 2 techniques performed similarly for identifying metastases (100.00% vs. 94.44% in lymph nodes, 100.00% vs. 87.50% in bone, 100.00% vs. 71.43% in liver, 100.00% vs. 66.67% in other sites, respectively). Significant differences were observed between SUV_{max} for ^{18}F-PFPN and SUV_{max} for ^{18}F-FDG measured at 1 and 3 h for both primary lesions ($P = 0.022$ and 0.008, respectively) and lymph node metastases ($P = 0.043$ and 0.005, respectively), with the former tracer showing the higher uptake.

On a lesion-based analysis, ^{18}F-PFPN PET/MRI detected a higher number of lesions than did ^{18}F-FDG PET (365 additional lesions); the detection rates according to the anatomic distribution were as follows: lymph nodes (100.00% vs. 79.03%, respectively), bone (100.00% vs. 38.32%, respectively), liver (100.00% vs. 34.75%, respectively), and other sites (100.00% vs. 87.88%, respectively). The SUV_{max} for ^{18}F-PFPN in the primary lesions, as well as in nodal, bone, and hepatic metastases, significantly increased from 1 to 3 h after injection ($P < 0.05$); conversely, a significant decrease was observed for most tissues and organs. A similar increase in normalized SUV_{max} for ^{18}F-PFPN was evident between 1 and 3 h. Notably, normalized SUV_{max} for ^{18}F-PFPN at 3 h was higher than that for ^{18}F-FDG for most lesions ($P < 0.01$). The original SUV_{max} data are shown in Supplemental Table 3.

On the visual scoring system (Fig. 3), ^{18}F-PFPN outperformed ^{18}F-FDG for the detection of distant metastases to the liver (10′ vs. 0′), bone (8′ vs. 0′), other distant sites (3′ vs. 0′) and lymph nodes (8′ vs. 0′). The total scores for ^{18}F-PFPN and ^{18}F-FDG PET were 29′ and 0′, respectively.

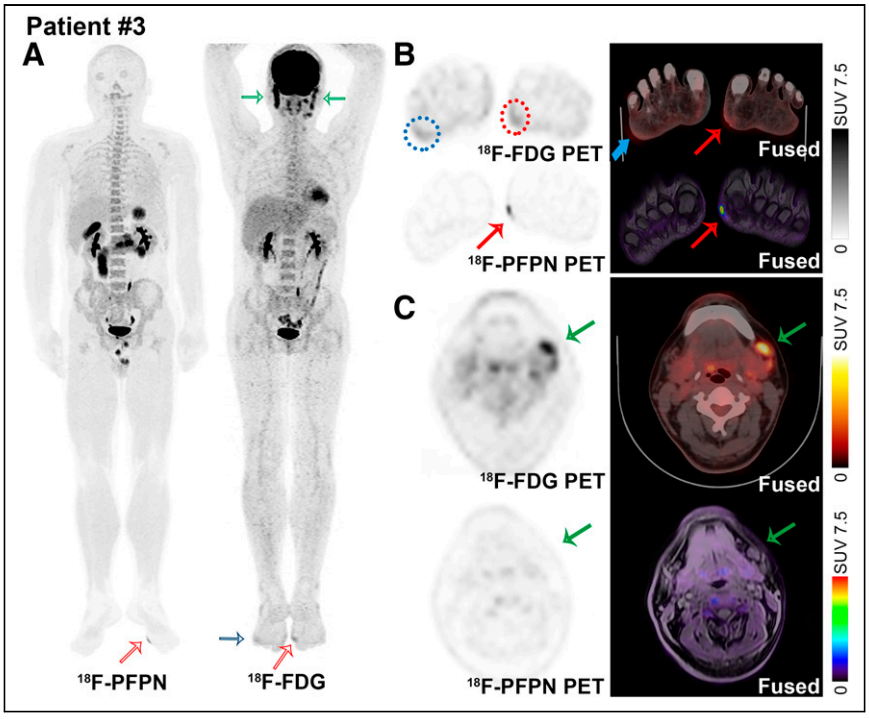

FIGURE 6. A 40-y-old man who sought medical attention for growing pigmented lesion on arch of left foot. ^{18}F-FDG PET images (A and B) revealed mild tracer accumulations in left anterior arch (red circle and red arrows; SUV_{max}, 3.3) and lateral margin of right foot (blue circle and blue arrows; SUV_{max}, 2.7). ^{18}F-PFPN PET clearly delineated left-foot lesion, which showed avid tracer uptake (SUV_{max}, 5.0), but ^{18}F-PFPN PET did not identify any lesion in right foot. Results of pathologic examination identified left-foot lesion as nodular ulcerated MM (thickness, 1.2 mm; pathologic T stage, pT2b). Interestingly, there was intense ^{18}F-FDG uptake in cervical lymph nodes (C, green arrows: SUV_{max}, 3.0–12.6), which, however, did not show significant ^{18}F-PFPN uptake. Collectively, these findings ruled out possibility that these lesions were metastases from MM; ^{18}F-FDG PET–positive nodes likely had reactive inflammatory nature.

Illustrative Case Reports

A 47-y-old man (patient 8, Fig. 4) underwent ^{18}F-PFPN PET for the detection of MM recurrences. ^{18}F-PFPN PET identified more lesions than ^{18}F-FDG PET did (fold-change in lesion detection for ^{18}F-PFPN PET: 2-fold higher for nodal metastases, 3-fold higher for hepatic metastases, and 2.5-fold higher for bone metastases). Notably, ^{18}F-PFPN PET successfully detected lesions smaller than 2 mm.

In patient 16 (Fig. 5), high background activity caused by elevated physiologic tracer uptake in the brain prevented the identification of cerebral metastases on ^{18}F-FDG PET imaging; however, the lesions were clearly visible on ^{18}F-PFPN PET images. Besides, MRI sequences provided diagnostic confirmation.

In patient 3 (Fig. 6), ^{18}F-PFPN PET, but not ^{18}F-FDG PET, correctly identified the

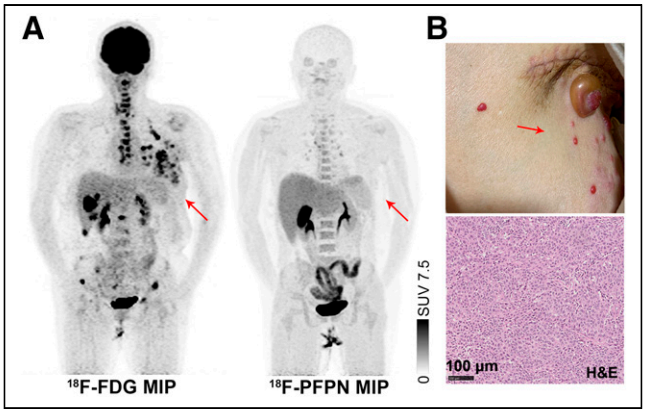

FIGURE 7. A 51-y-old woman who underwent partial excision of MM in left breast 1 y before PET imaging. She was regularly followed up; marked increase in serum CA 19-9 level (>1,200 U/mL; reference range, 0–35 U/mL) was evident over last 4 mo. (A) On ^{18}F-FDG PET imaging, avid tracer uptake was evident in operated breast (SUV_{max}, 3.7–10.4), axillary lymph nodes (SUV_{max}, 3.8–9.6), and bone (SUV_{max}, 3.2–10.2), indicating recurrent disease. Unexpectedly, ^{18}F-PFPN PET imaging findings were negative. (B) Visual examination of operated breast showed nonpigmented recurrent lesions. Pathology examination (hematoxylin and eosin [H&E] staining) of axillary lymph nodes identified metastases from MM; however, these metastatic cells were proven to be nonpigmented (unable to produce melanin). Red arrows indicate breast lesion.

primary lesion located in the left foot as an early-stage melanoma. Interestingly, the cervical lymph nodes showed intense ^{18}F-FDG uptake, whereas there was no ^{18}F-PFPN accumulation in these areas. The follow-up results suggested the findings to be inflammatory but not metastasis lesions and false-positive on ^{18}F-FDG PET.

Figure 7 shows an illustrative case of ^{18}F-PFPN PET and ^{18}F-FDG PET findings in a woman with distant amelanotic lesions from MM. Melanoma cells unable to produce melanin were missed on ^{18}F-PFPN PET, which further confirmed the specificity of ^{18}F-PFPN as a melanin PET tracer.

DISCUSSION

There are 2 principal findings from this study. First, on analyzing the biodistribution, pharmacokinetics, radiation dosimetry, and safety of ^{18}F-PFPN in 5 healthy volunteers, we found that this melanin PET tracer was safe and well tolerated; also, its absorbed radiation dose was comparable to ^{18}F-FDG. Second, in a pilot clinical investigation on suspected or confirmed MM patients, ^{18}F-PFPN showed higher uptake than ^{18}F-FDG for both primary tumors and distant metastases. In a lesion-based analysis,^{18}F-PFPN PET imaging could detect 365 metastases that were missed on ^{18}F-FDG PET. Collectively, these data represent a promising step in understanding the clinical value of ^{18}F-PFPN PET imaging for diagnosing and detecting disease recurrences in MM.

Although ^{18}F-FDG PET imaging has extensive applications in patients with solid malignancies (*20*), its clinical value in MM is beset by high false-positive rates (100% in early-stage MM) (*21*). In this scenario, there have been increasing efforts to develop novel PET tracers capable of recognizing and binding to melanin with high affinity and specificity. The melanin PET tracer used in this study (^{18}F-PFPN) was optimized and improved on the basis of our previous nicotinamide probe, ^{18}F-5-FPN (*17*). Compared with the parent molecule, ^{18}F-PFPN is characterized by a more favorable pharmacokinetic profile—importantly, the negligible hepatic accumulation and rapid renal clearance (*19*)—thus endowing this tracer with the capacity to be safely applied for clinical imaging studies.

However, partial excretion may occur through the hepatobiliary system, which may at least in part account for both gallbladder and intestinal wall uptake. On another note, the annular tracer accumulation in the eyes can be explained by the presence of choroidal melanocytes and retinal pigment cells. In terms of radiation safety, the total effective dose of ^{18}F-PFPN was 0.020 mSv/MBq, which is comparable to the whole-body effective dose of ^{18}F-FDG (0.019 mSv/MBq) (*22*). Collectively, these results prompted us to conduct the first clinical ^{18}F-PFPN PET imaging study in patients with MM.

First, on analyzing diagnostic performance for the detection of primary MM, we found that ^{18}F-PFPN PET could identify early T-stage lesions (e.g., T2b). Additionally, significant differences were observed between SUV_{max} for ^{18}F-PFPN and SUV_{max} for ^{18}F-FDG measured at 3 h for primary lesions, with the former tracer showing the highest uptake (3.92-fold higher uptake than that of ^{18}F-FDG). In view of these findings, we subsequently examined the role of ^{18}F-PFPN PET imaging to identify distant metastases. Although the results of ^{18}F-PFPN PET imaging led to modifications in disease staging for one patient only (1/9), this may be related to the high proportion of patients with advanced disease stages. Interestingly, ^{18}F-PFPN showed low background activity, ultimately allowing reliable delineation of a higher number of distant lesions from MM, including those at nodal, bone, and hepatic sites. Pigmented lesions can appear hyperintense on T1-weighted MR images because of the high number of negative melanin charges, which ultimately facilitate iron binding. In this scenario, the combination of ^{18}F-PFPN PET with MRI can increase image interpretation accuracy. Immune checkpoint inhibitions could enhance immune cells to kill tumors, which had been one of the main treatments for metastatic melanoma (*23*). ^{18}F-PFPN may provide an excellent possibility to distinguish between inflammatory processes and melanotic lesions through specific binding to melanin. Benefitting from this capacity, ^{18}F-PFPN imaging could be a valuable tool to evaluate immune checkpoint inhibition efficacy by reflecting the changes in melanoma tumor cells. However, ^{18}F-PFPN PET may underperform traditional ^{18}F-FDG PET in less common amelanotic or hypomelanotic subtypes of MM, which comprise 2%−8% of all cases. These lesions, whose appearance can mimic several benign and malignant conditions, continue to pose significant diagnostic challenges (*11*).

Our findings need to be interpreted in the context of some limitations. First, it would have been interesting to include patients with early-stage (I−II) MM; more research is necessary to confirm our findings and to evaluate the role of ^{18}F-PFPN PET imaging in this patient group. Second, our study focused on the clinical value of this imaging modality in patients with pigmented MM. One of the study patients had her distant amelanotic lesions missed on ^{18}F-PFPN PET; therefore, the possibility of nonpigmented lesions in patients with MM should be based on a comprehensive consideration of thorough clinical and imaging investigations. Finally, the single-center design may have limited the external validity of our results. Despite these limitations, our data represent a promising step in understanding the potential utility of ^{18}F-PFPN as a melanin tracer and may open new research directions. For example, labeling ^{18}F-PFPN with therapeutic radioisotopes may warrant further scrutiny as a potential therapeutic strategy in metastatic MM (*24*).

CONCLUSION

^{18}F-PFPN is a safe and well-tolerated melanin PET tracer. In a pilot clinical study, ^{18}F-PFPN PET outperformed traditional ^{18}F-FDG PET in identifying both primary MM and distant metastases. Further research is needed to verify these results in a larger sample and investigate the clinical value of ^{18}F-PFPN PET imaging in early-stage MM.

DISCLOSURE

This work was financially supported by the National Natural Science Foundation of China (grants 81901783 and 82030052). Tzu-Chen Yen is an employee of Aprinoia Therapeutics Co., Ltd. No other potential conflict of interest relevant to this article was reported.

ACKNOWLEDGMENT

We thank Chunxia Qin for technical assistance.

KEY POINTS

QUESTION: ^{18}F-PFPN is a novel PET probe with high affinity and selectivity for melanin; it may have clinical utility in patients with MM.

PERTINENT FINDINGS: In MM patients, uptake of ^{18}F-PFPN was higher than that of ^{18}F-FDG for both primary tumors and metastases, and ^{18}F-PFPN PET could detect 365 metastases missed on ^{18}F-FDG PET. Additionally, ^{18}F-PFPN PET had clinical value in distinguishing false-positive lesions on ^{18}F-FDG PET.

IMPLICATIONS FOR PATIENT CARE: ^{18}F-PFPN PET may outperform traditional ^{18}F-FDG PET in identifying both primary melanoma and its distant spread.

REFERENCES

1. Siegel RL, Miller KD, Fuchs HE, Jemal A. Cancer statistics, 2021. *CA Cancer J Clin.* 2021;71:7–33.
2. Schüle SC, Eigentler TK, Garbe C, la Fougere C, Nikolaou K, Pfannenberg C. Influence of ^{18}F-FDG PET/CT on therapy management in patients with stage III/IV malignant melanoma. *Eur J Nucl Med Mol Imaging.* 2016;43:482–488.
3. Stelter L, Evans MJ, Jungbluth AA, et al. Novel mechanistic insights into arginine deiminase pharmacology suggest ^{18}F-FDG is not suitable to evaluate clinical response in melanoma. *J Nucl Med.* 2012;53:281–286.
4. Wagner JD, Schauwecker D, Davidson D, et al. Inefficacy of F-18 fluorodeoxy-D-glucose-positron emission tomography scans for initial evaluation in early-stage cutaneous melanoma. *Cancer.* 2005;104:570–579.
5. Cheng Z, Zhang L, Graves E, et al. Small-animal PET of melanocortin 1 receptor expression using a ^{18}F-labeled α-melanocyte-stimulating hormone analog. *J Nucl Med.* 2007;48:987–994.
6. Revskaya E, Jongco AM, Sellers RS, et al. Radioimmunotherapy of experimental human metastatic melanoma with melanin-binding antibodies and in combination with dacarbazine. *Clin Cancer Res.* 2009;15:2373–2379.
7. Jandl T, Revskaya E, Jiang Z, Bryan RA, Casadevall A, Dadachova E. Complement-dependent cytotoxicity of an antibody to melanin in radioimmunotherapy of metastatic melanoma. *Immunotherapy.* 2013;5:357–364.
8. Gao F, Sihver W, Jurischka C, et al. Radiopharmacological characterization of ^{64}Cu-labeled α-MSH analogs for potential use in imaging of malignant melanoma. *Amino Acids.* 2016;48:833–847.
9. Beaino W, Anderson CJ. PET imaging of very late antigen-4 in melanoma: comparison of ^{68}Ga- and ^{64}Cu-labeled NODAGA and CB-TE1A1P-LLP2A conjugates. *J Nucl Med.* 2014;55:1856–1863.
10. Wei W, Ehlerding EB, Lan X, Luo Q, Cai W. PET and SPECT imaging of melanoma: the state of the art. *Eur J Nucl Med Mol Imaging.* 2018;45:132–150.
11. Thomas NE, Kricker A, Waxweiler WT, et al. Comparison of clinicopathologic features and survival of histopathologically amelanotic and pigmented melanomas: a population-based study. *JAMA Dermatol.* 2014;150:1306–1314.
12. Liu X, Pham TQ, Berghofer P, et al. Synthesis and evaluation of novel radioiodinated nicotinamides for malignant melanoma. *Nucl Med Biol.* 2008;35:769–781.
13. Ma X, Wang S, Wang S, et al. Biodistribution, radiation dosimetry, and clinical application of a melanin-targeted PET probe, ^{18}F-P3BZA, in patients. *J Nucl Med.* 2019;60:16–22.
14. Rizzo-Padoin N, Chaussard M, Vignal N, et al. [^{18}F]MEL050 as a melanin-targeted PET tracer: fully automated radiosynthesis and comparison to ^{18}F-FDG for the detection of pigmented melanoma in mice primary subcutaneous tumors and pulmonary metastases. *Nucl Med Biol.* 2016;43:773–780.
15. Garg PK, Nazih R, Wu Y, Singh R, Garg S. 4-^{11}C-methoxy *N*-(2-diethylaminoethyl) benzamide: a novel probe to selectively target melanoma. *J Nucl Med.* 2017;58:827–832.
16. Liu M, Wang Y, Li M, et al. Using tyrosinase as a tri-modality reporter gene to monitor transplanted stem cells in acute myocardial infarction. *Exp Mol Med.* 2018;50:1–10.
17. Feng H, Xia X, Li C, et al. Imaging malignant melanoma with ^{18}F-5-FPN. *Eur J Nucl Med Mol Imaging.* 2016;43:113–122.
18. Wang Y, Li M, Zhang Y, et al. Detection of melanoma metastases with PET: comparison of ^{18}F-5-FPN with ^{18}F-FDG. *Nucl Med Biol.* 2017;50:33–38.
19. Xu X, Yuan L, Yin L, et al. Synthesis and preclinical evaluation of ^{18}F-PEG$_3$-FPN for the detection of metastatic pigmented melanoma. *Mol Pharm.* 2017;14:3896–3905.
20. Groheux D, Cochet A, Humbert O, Alberini JL, Hindié E, Mankoff D. ^{18}F-FDG PET/CT for staging and restaging of breast cancer. *J Nucl Med.* 2016;57(suppl 1):17S–26S.
21. Acland KM, Healy C, Calonje E, et al. Comparison of positron emission tomography scanning and sentinel node biopsy in the detection of micrometastases of primary cutaneous malignant melanoma. *J Clin Oncol.* 2001;19:2674–2678.
22. Liu T, Liu C, Zhang Z, et al. ^{64}Cu-PSMA-BCH: a new radiotracer for delayed PET imaging of prostate cancer. *Eur J Nucl Med Mol Imaging.* 2021;48:4508–4516.
23. Dummer R, Lebbé C, Atkinson V, et al. Combined PD-1, BRAF and MEK inhibition in advanced BRAF-mutant melanoma: safety run-in and biomarker cohorts of COMBI-i. *Nat Med.* 2020;26:1557–1563.
24. Xu X, Yuan L, Gai Y, et al. Targeted radiotherapy of pigmented melanoma with ^{131}I-5-IPN. *J Exp Clin Cancer Res.* 2018;37:306.